De Novo Proteins as Models of Radical Enzymes†

Cecilia Tommos, Jack J. Skalicky,‡ Denis L. Pilloud, A. Joshua Wand, and P. Leslie Dutton*

The Johnson Research Foundation, Department of Biochemistry and Biophysics, University of Pennsylvania, Philadelphia, Pennsylvania 19104

Received March 17, 1999

ABSTRACT: Catalytically essential side-chain radicals have been recognized in a growing number of redox enzymes. Here we present a novel approach to study this class of redox cofactors. Our aim is to construct a de novo protein, a radical maquette, that will provide a protein framework in which to investigate how side-chain radicals are generated, controlled, and directed toward catalysis. A tryptophan and a tyrosine radical maquette, denoted α_3W^1 and α_3Y^1, respectively, have been synthesized. α_3W^1 and α_3Y^1 contain 65 residues each and have molecular masses of 7.4 kDa. The proteins differ only in residue 32, which is the position of their single aromatic side chain. Structural characterization reveals that the proteins fold in water solution into thermodynamically stable, α-helical conformations with well-defined tertiary structures. The proteins are resistant to pH changes and remain stable through the physiological pH range. The aromatic residues are shown to be located within the protein interior and shielded from the bulk phase, as designed. Differential pulse voltammetry was used to examine the reduction potentials of the aromatic side chains in α_3W^1 and α_3Y^1 and compare them to the potentials of tryptophan and tyrosine when dissolved in water. The tryptophan and tyrosine potentials were raised considerably when moved from a solution environment to a well-ordered protein milieu. We propose that the increase in reduction potential of the aromatic residues buried within the protein, relative to the solution potentials, is due to a lack of an effective protonic contact between the aromatic residues and the bulk solution.

A family of redox proteins that employs amino acids, or posttranslationally modified amino acids, as active, electron-transfer cofactors has recently been recognized (*1*−*6*). The side-chain cofactors in this class of enzymes include tyrosine, tryptophan, cysteine, glycine, and derivatives of tyrosine and tryptophan. The tyrosyl radical in the iron-containing ribonucleotide reductase (RNR)[1] enzyme involved in DNA synthesis was the first functional protein radical that was shown to reside on a side chain (*1*, *7*). Over the past two decades, amino acid radicals have been shown to participate in a number of biochemical reactions including water oxidation in plants and algae, carbohydrate metabolism, hormone synthesis, and deactivation of reactive oxygen species in the cell (*4*−*6*). Interestingly, a postulated redox-active tyrosine, located in the binuclear center in cytochrome *c* oxidase and cross-linked to a histidine (*8*, *9*), has recently been proposed to participate in the reduction of oxygen in respiration (*10*).

The use of side chains as catalytic cofactors raises mechanistic questions as to how these amino acids specifically are targeted for redox chemistry. One theme emerging for the enzymes studied thus far is the presence of a metal site in the immediate vicinity of the redox-active side chain that generates the oxidizing potential necessary to form the catalytically active radical. The metal cofactors involved in radical generation are diverse and include most of the redox-active metals commonly found in natural systems. Oxygen-activated heme and non-heme iron are essential for radical formation in cytochrome *c* peroxidase (*11*) and in the class Ia RNR enzymes (*12*), respectively. Cobalt is present in the B_{12}-dependent proteins (*2*, *4*, *6*). Mononuclear copper centers are found in, for example, galactose oxidase (*13*), and a manganese cofactor has been proposed to form the metal site in the class Ib RNR enzymes (*14*, *15*). An iron−sulfur cluster and *S*-adenosylmethionine are required for the formation of the stable glycine radicals found in the anaerobic pyruvate formate lyase (*16*) and class III RNR (*17*) enzymes. In these two latter proteins, the metal and the radical are located on separate subunits. Photosystem II (PSII) of plant photosynthesis provides another exception to the close metal/radical motif described above. In this system, a light-activated chlorophyll complex, P680, generates the potential to oxidize two tyrosines, denoted Y_Z and Y_D, in which the former is

† This work was funded by the National Institutes of Health (Grants GM 48130 to P.L.D. and GM 35940 to A.J.W.) and in part by the National Science Foundation (Grant MRSEC IRG DMR96-32598 to P.L.D.). J.J.S. was supported by a National Service Research Award (Grant GM 18121). C.T. gratefully acknowledges a postdoctoral fellowship from the Swedish Foundation for International Cooperation in Research and Higher Education.

* Corresponding author: B501 Richards Building, Department of Biochemistry and Biophysics, University of Pennsylvania, Philadelphia, PA 19104; phone (215) 898-5668; fax (215) 573-2235; e-mail dutton@mail.med.upenn.edu.

‡ Present address: Department of Chemistry, State University of New York, Buffalo, NY 14260.

[1] Abbreviations: 1D and 2D, one- and two-dimensional; α_3W^1, a de novo protein containing a single buried tryptophan; α_3Y^1, a de novo protein containing a single buried tyrosine; ANS, 8-anilino-1-naphthalenesulfonic acid; CD, circular dichroism; DPV, differential pulse voltammetry; E_m, midpoint potential; E_P, peak potential; HSQC, heteronuclear single quantum coherence; IP, ionization potential; NHE, normal hydrogen electrode; NMR, nuclear magnetic resonance; NOE, nuclear Overhauser enhancement; NOESY, nuclear Overhauser enhancement spectroscopy; PSII, photosystem II; RNR, ribonucleotide reductase; Y_Z and Y_D, redox-active tyrosines in photosystem II.

10.1021/bi990609g CCC: $18.00
Published on Web 06/29/1999

directly involved in the water-oxidizing chemistry (*18*, *19*). In several of the radical enzymes it appears that the principal, and in some systems the sole, function of the metal is to generate the potential required to oxidize the side-chain cofactor. Once created, the radical then interacts with the substrate to initiate catalysis.

A distinct feature of redox-active amino acids is that they change their acidity dramatically as a function of their redox state. Tyrosine, for example, has a solution p*K* of 10, which is lowered by more than 12 p*K* units upon oxidation (*20*). Similarly, tryptophan has a p*K* above 14 in its reduced form that drops to about 4 in its oxidized radical form (*21*, *22*). Radical-driven deprotonation and reprotonation reactions are often part of the catalytic cycle in this class of enzymes (*4*−*6*). In recent models for PSII, for example, redox-coupled proton exchange at Y_Z has been proposed to serve as the key mechanism by which the protons produced by the water-oxidizing chemistry are shuttled from the catalytic site to the bulk solution in the thylakoid lumen (*19*, *23*).

Some enzymes generate and confine the radical at the active site. In contrast, in the RNR enzymes the initial radical is generated at a position remote from the site of catalysis and radical migration in a controlled fashion is invoked in substrate activation (*6*, *12*, *24*−*26*). Pyruvate formate lyase provides a second example in which radical migration is proposed to occur (*27*, *28*). Side-chain redox reactions typically occur at high reduction potentials and involve exchange of single electrons, making the radical state a powerful and highly reactive oxidant. The high reactivity, combined with the apparent ease by which side-chain radicals migrate in physiological reactions, suggests that the proteins that support functional radicals contain features to exert strict control on the reactive species so as not to damage the host organism.

It is of considerable interest and importance to delineate the general engineering principles by which the protein controls the formation of the radical, prevents destructive side reactions, and moves it with high efficiency toward the substrate. Here we describe a novel approach to investigate these issues. Our aim is to construct a radical maquette that will serve as a working model for the family of radical enzymes. The radical maquette is a de novo designed protein containing a buried amino acid that is targeted for redox chemistry. In the design of the first generation of radical maquettes, our emphasis was to develop a protein framework that satisfies four basic criteria: (1) The synthetic protein should have structural properties similar to those of natural proteins and thus form stable, well-defined secondary and tertiary structures in solution. (2) The protein should contain a single side-chain cofactor located within the protein core and shielded from the bulk solution. Our intention is to study the interplay between the protein and the radical. Therefore, the side-chain cofactor should be buried within the protein interior, rather than located in a solvent-exposed position in which solution conditions are expected to dominate its chemistry. (3) To provide a stabilizing environment and suppress possible side reactions, the rest of the protein should be "redox inert" and not contain residues expected to have reduction potentials close to that of the endogenous cofactor. (4) The protein scaffold should have a small extinction coefficient in the region in which the amino acid cofactor absorbs. This feature is intended to allow us to photooxidize the side-chain cofactor specifically without initiating additional light-induced reactions.

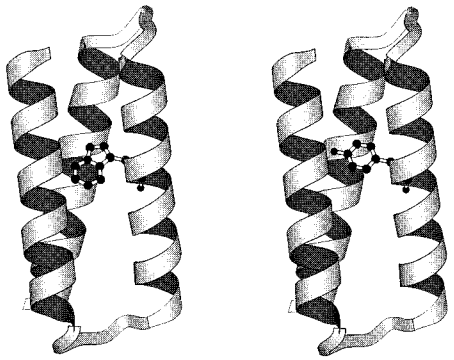

FIGURE 1: Structural models of the tryptophan and tyrosine radical maquettes, denoted α_3W^1 and α_3Y^1. The figures were generated by MOLSCRIPT (*29*) and are based on the crystal coordinates of CoilSer designed by DeGrado and co-workers (*30*).

We have constructed two small globular proteins that include either a single tryptophan or a single tyrosine based on these principles. Structural models of the tryptophan and tyrosine radical maquettes, denoted α_3W^1 and α_3Y^1, are shown in Figure 1. Here we present a detailed evaluation of the solution properties of the two synthetic proteins and of the local environment of their aromatic side chains. This work provides experimental support for the models shown in Figure 1. Following the structural characterization, the electrochemical properties of α_3W^1 and α_3Y^1 were examined and these results begin to identify features essential to generate side-chain radicals within the interior of a protein.

EXPERIMENTAL PROCEDURES

Materials. 9-Fluorenylmethoxycarbonyl (Fmoc) protected amino acid pentafluorophenyl esters (OPfp) were obtained from PerSeptive Biosystems (Framingham, MA) except for Fmoc-Arg(Pmc)-OPfp, which was purchased from Bachem (King of Prussia, PA). NovaSyn PR 500 resin was obtained from Calbiochem−Novabiochem (La Jolla, CA), trifluoroacetic acid (TFA) and 2,2,2-trifluoroethanol (TFE) from Aldrich Chemical Co. (Milwaukee, WI), and 1,2-ethanedithiol and 1-hydroxybenzotriazole (HOBt) from Fluka (Ronkonkoma, NY). L-Tyrosine, *N*-acetyl-L-tyrosinamide, and *N*-acetyl-L-tryptophanamide were obtained from Sigma Chemical Co. (St. Louis, MO). All chemicals and solvents were reagent-grade and were used as received. The water used was purified in a Milli-Q system from Millipore Corp. (Bedford, MA).

Protein Synthesis. The α_3W^1 and α_3Y^1 peptide chains, *acetyl*-R·VKALEEK·VKALEEK·VKAL-*GGGG*-R·IEELKKK·(**W**/**Y**)EELKKK·IEEL-*GGGG*-E·VKKVEEE·VKKLEEE·IKKL-*CONH*$_2$, were assembled on a continuous-flow MilliGen 9050 solid-phase synthesizer by using Fmoc-protected L-amino acids on a 0.2 mmol scale. The side-chain protecting groups were as follows: Arg (2,2,5,7,8-pentamethylchroman-6-sulfonyl), Glu (*tert*-butyl ester), Lys (*tert*-butyloxycarbonyl), Tyr (*tert*-butyl). Single, 60 min cycles were used for the OPfp/HOBt coupling steps with the exception of Ala, which was double-coupled. After synthesis, the N-termini were acetylated in acetic anhydride/pyridine 1:1 (v/v) for 30 min and then rinsed with *N*,*N*-dimethylformamide followed by dichloromethane. The synthesized

peptides were cleaved from the solid resin support and their side chains were concomitantly deprotected in a TFA/1,2-ethanedithiol/water 90:8:2 (v/v/v) mixture for 4.5 h. The resin was filtered and the crude products were precipitated and washed in ether and then dissolved in water with 0.1% TFA. After lyophilization, the peptides were purified by reversed-phase HPLC on a C18 column (Vydac, Hesperia, CA) eluted with an acetonitrile/water/0.1% TFA gradient. The purity of the final products was assayed by analytical HPLC and their molecular masses, 7440 and 7417 Da for α_3W^1 and α_3Y^1, respectively, were verified by mass spectroscopy. Protein concentrations were determined in 6 M guanidine hydrochloride (GdnHCl) and assuming ϵ_{280} of 5690 M^{-1} cm^{-1} for tryptophan and ϵ_{275} of 1490 M^{-1} cm^{-1} for tyrosine (*31*).

Solution Molecular Weight Determination. Sedimentation equilibrium ultracentrifugation was performed as described earlier (*32*). The protein concentration was 150 μM in a buffer of 10 mM potassium phosphate and 100 mM KCl, pH 7.0. Analytical size-exclusion chromatography was done by using a Pharmacia Superdex 75 column equilibrated with the buffer described above at a flow rate of 0.5 mL min^{-1}. The protein loading concentration was 4−850 μM and the eluent was monitored by measuring the absorbance at 220 and 280 nm.

Circular Dichroism Spectroscopy. CD measurements were performed on an Aviv 62DS spectropolarimeter at 25.0 °C by using a 2 mm path length cuvette. CD intensity is expressed as mean residue ellipticity [Θ] (degree square centimeter per decimole), which is given by $[\Theta] = \Theta_{obs}/10lCn$, where Θ_{obs} is the measured ellipticity in degrees, l is the cuvette path length in centimeters, C is the molar peptide concentration, and n represents the number of amino acids. The chemical denaturation curves were obtained by monitoring the ellipticity at 222 nm as a function of GdnHCl concentration. The denaturation data were fit to a two-state monomer folded/unfolded equilibrium, fraction folded $= \exp(\Delta G^{H_2O} - m[\text{GdnHCl}])/\{1 + \exp(\Delta G^{H_2O} - m[\text{GdnHCl}])\}$, by using a nonlinear least-squares routine in KaleidaGraph (Synergy Software, Reading, PA). The ΔG^{H_2O} term represents the free energy of unfolding in the absence of denaturant and the m value, the slope of the denaturation curve, reflects the degree of cooperativity in the unfolding process (*33*).

NMR Spectroscopy. NMR experiments were performed on a Varian Inova 600 or 750 MHz spectrometer. α_3W^1 and α_3Y^1 solutions were prepared at 1 mM concentration in 20 mM sodium phosphate, pH 7.0, 50 mM KCl, 0.01 mM sodium azide, and a H_2O:D_2O ratio of 94:6 (v/v). One-dimensional NMR spectra were acquired with a 12 ppm spectral width and 4096 complex data points. Two-dimensional NOESY (*34*) experiments were acquired with a 12.0 ppm spectral width in $t_1(^1H)$ and $t_2(^1H)$, acquiring 300 and 2048 complex points in each dimension, with a total acquisition times of 41.7 and 284 ms, respectively. Natural abundance ^{13}C HSQC (*35*, *36*) spectra were acquired with a 31.8 ppm spectral width in $t_1(^{13}C)$ with 140 complex points (29.2 ms total acquisition time) and 12.0 ppm spectral width in $t_2(^1H)$ with 2048 complex points (284 ms total acquisition time). Quadrature detection in the indirect dimensions was accomplished by using TPPI−States (*37*). Data reduction was performed with Felix95 software (Molecular Simulations Inc., San Diego, CA). Amide H/D isotope exchange (*38*) was performed by dissolving perprotio α_3W^1 or α_3Y^1 in 99.9% D_2O and immediately placing the samples in the NMR spectrometer. Following 15 min equilibration time, the rate of amide hydrogen exchange of the slowest hydrogens was monitored with a series of one-dimensional NMR spectra.

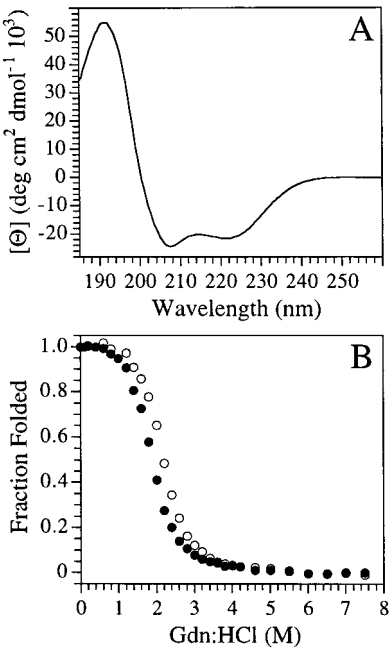

FIGURE 2: (A) Circular dichroism spectrum of α_3Y^1 at neutral pH. (B) Reversible guanidine hydrochloride denaturation of α_3W^1 (○) and α_3Y^1 (●) as monitored by their CD intensities at 222 nm. The proteins were dissolved at 13.0 μM in 10 mM potassium phosphate and 10 mM KCl, pH 7.0. The data were collected at 25 °C.

Electrochemical Measurements. Differential pulse voltammetry (DPV) measurements were done on a BAS 100 B/W electrochemical analyzer from Bioanalytical Systems (West Lafayette, IN). The data were collected in a three-electrode glass cell by using a glassy carbon working electrode, an Ag/AgCl/3 M KCl reference electrode, and a platinum wire as the counter electrode. The glassy carbon electrode was polished with a water−alumina slurry, rinsed, and sonicated between each single measurement. The free amino acids and the proteins were dissolved in a 10 mM potassium phosphate buffer containing 200 mM KCl. The pH was set by using stock solutions of HCl and KOH and monitored continuously during the experiments. The sample volumes were 3 mL, from which oxygen was removed by passing wet argon gas either above or through the solution prior to each measurement. The experiments were performed at 22 °C. The ferricyanide/ferrocyanide redox couple was used as an internal standard. All potentials reported here are presented relative to the normal hydrogen electrode (NHE).

RESULTS

Folding of α_3W^1 and α_3Y^1. The secondary structures of α_3W^1 and α_3Y^1 were studied by CD and NMR spectroscopies. Figure 2A displays the far-UV spectrum of α_3Y^1 in aqueous buffer, which shows the positive 192 nm and negative 208 and 222 nm features characteristic of an α-helical backbone structure (*39*). The α_3Y^1 CD spectrum displays a mean residue ellipticity at 222 nm, $[\Theta]_{222}$, of -21.5 10^3 deg cm^2 $dmol^{-1}$ and a $[\Theta]_{222}/[\Theta]_{208}$ ratio of 0.89. These values are consistent with a protein structure of

interacting α-helices (*40*, *41*). The $[\Theta]_{222}$ and $[\Theta]_{222}/[\Theta]_{208}$ values decreased to −24.3 10^3 deg cm^2 dmol^{-1} and 0.81 when α_3Y^1 was dissolved in buffer containing 50% trifluoroethanol (not shown). Trifluoroethanol is a more hydrophobic solvent and a weaker base as compared to water. When added at high concentrations, TFE disrupts the protein hydrophobic core and stabilizes intrahelical hydrogen bonds, which promotes helix formation in peptides with helical propensity (*42*−*44*). The formation of monomeric α-helices in the presence of TFE is consistent with the decrease to 0.81 in the $[\Theta]_{222}/[\Theta]_{208}$ ratio (*40*, *41*). The relatively minor change observed in the CD intensity at 222 nm upon TFE addition indicates that the backbone folding in α_3Y^1 is essentially complete in an aqueous milieu. α_3W^1 gives rise to very similar CD spectra as compared to α_3Y^1 in both aqueous and TFE-containing buffers (not shown). We estimate that the two proteins are ∼70% α-helical in water from their CD spectra (*45*).

Nuclear magnetic resonance studies also indicate that α_3W^1 and α_3Y^1 are helical, as designed. Most of the resonances of the backbone H^α nuclei are observed in the 3.8−4.3 ppm region in the one-dimensional ^{1}H NMR spectra of α_3W^1 and α_3Y^1 (not shown). These values are shifted upfield, as compared to random-coil values (*46*, *47*), which is consistent with resonances of H^α nuclei in α-helices (*48*). Furthermore, 2D NOESY spectra from α_3W^1 and α_3Y^1 (not shown) reveal numerous H^N-H^N correlations, as expected for α-helical proteins.

The thermodynamic stability of α_3W^1 and α_3Y^1, relative to their unfolded states, was studied by chemical denaturation and amide H/D isotope exchange measurements. Figure 2B shows the reversible loss of their secondary structure, probed by the decrease in ellipticity at 222 nm, as a function of guanidine hydrochloride concentration. The denaturation curves have a midpoint of unfolding at 2.2 and 1.9 M GdnHCl for α_3W^1 and α_3Y^1, respectively. Figure 2B shows that the secondary structures of α_3W^1 and α_3Y^1 melt in a very cooperative manner. The two denaturation transitions have *m* values of 2.8 kcal mol^{-1} M^{-1}, which is consistent with values derived for natural proteins (*49*). Assuming a two-state monomer folded/unfolded event, we estimate ΔG^{H_2O} at 25 °C to be −6.2 kcal mol^{-1} for α_3W^1 and −5.4 kcal mol^{-1} for α_3Y^1. The slowest amide H/D exchange rate translates to a range of ΔG^{H_2O} that includes the value measured by chemical denaturation. The rate of the slowest exchanging amide proton in α_3W^1 is 0.0085 min^{-1} at pH 6.85 (uncorrected for isotope effects) and 25 °C. This equates to a free energy of unfolding of −5.1 to −6.3 kcal mol^{-1} depending upon its identity (*50*, *51*). Likewise, the rate of the slowest exchanging amide proton in α_3Y^1 is 0.0025 min^{-1} at pH 6.50 (uncorrected for isotope effects) and 25 °C. This equates to a ΔG^{H_2O} value of −5.4 to −6.5 kcal mol^{-1}. Thus, the stability of α_3W^1 and α_3Y^1 as determined by amide H/D exchange is consistent with the chemical denaturation measurements and further suggests that the rate of the slowest exchanging amide proton is being controlled by a global unfolding event (*51*).

The radical maquettes are somewhat more stable than the original molecule, denoted α_3-1 (*30*, *32*), from which their sequences were derived. α_3-1 displays a ΔG^{H_2O} of −4.6 kcal mol^{-1} at 25 °C (*32*). The thermodynamic stability of the de novo α_3B and α_3C three-helix bundles, −7.2 and −5.5 kcal mol^{-1}, respectively (*52*), is close to the values that we observe for α_3W^1 and α_3Y^1. The stabilities of the radical maquettes are also close to values reported for natural proteins of similar size. Four single-stranded proteins or domains, containing between 56 and 65 residues and no S−S bridges, display stability in the range of −5.7 to −7.5 kcal mol^{-1} (*53*−*56*). The SH3 domain, which is a 62-residue, β-sheet barrel, displays a ΔG^{H_2O} of −3.7 kcal mol^{-1} (*57*). Thus, the thermodynamic stability of α_3W^1 and α_3Y^1 is within the range observed for other small, monomeric proteins of both synthetic and natural origin.

It is common that de novo proteins fold into well-defined backbone conformations but form less ordered tertiary structures (*58*−*61*). The synthetic proteins show features resembling molten globules, which are compact, partially folded conformations with mobile side chains (*62*). The steep melting transitions shown in Figure 2B indicate that the unfolding processes of α_3W^1 and α_3Y^1 are highly cooperative events. This, in turn, suggests that these two proteins form rigid and well-ordered hydrophobic cores that are shielded from bulk solvent. To test this, we studied binding of the amphipathic fluorescent dye 8-anilino-1-naphthalenesulfonic acid (ANS) to α_3W^1 and α_3Y^1. Proteins with poorly packed interiors typically have a high affinity for ANS, the binding of which can be monitored spectroscopically (*63*). When excited with 370 nm light, ANS has a low fluorescence yield in water but gives rise to a strong emission in the 450−550 nm region when residing in a hydrophobic environment. We observed no increase in fluorescence in this region upon addition of α_3W^1 or α_3Y^1 to a neutral solution containing 11.4 μM ANS (not shown). We conclude that these two proteins do not bind ANS in a solution containing a 1:1 ratio of dye and protein, which is consistent with tightly packed tertiary structures.

NMR studies were performed to establish further that α_3W^1 and α_3Y^1 have well-defined folds in solution. An NMR spectrum displaying narrow resonance line widths, large chemical-shift dispersion, and a single set of resonances is characteristic of a well-folded protein in solution. Multiplicity of solution conformations and the rates of interchange, relative to the chemical shift differences, between these conformers will have dramatic effects on the magnetic resonances. Slow exchange rates will lead to observation of individual resonances of each conformation that is population-weighted in intensity. Thus, a protein that populates a manifold of slowly interchanging conformations will exhibit multiple and/or broadened magnetic resonances. A situation with intermediate exchange rates will result in extreme line broadening. Rapid exchange between different conformers will lead to a population-weighted average chemical shift with a more narrow dispersion range. The isotropic magnetic environment and resulting small range of chemical-shift dispersion in random coils exemplifies this latter situation.

Figure 3 shows one-dimensional ^{1}H NMR spectra containing resonances of main-chain amide and aromatic protons in α_3W^1 (panel A) and α_3Y^1 (panel B). Both spectra show amide proton resonances spanning a ∼2 ppm region that display narrow line widths. The chemical shift dispersion predicted for the amide protons associated with the α_3W^1 and α_3Y^1 peptide chains in a random-coil conformation is about 0.4 ppm (*46*, *47*). The much larger range in chemical shifts observed in the two spectra indicates that the α_3W^1

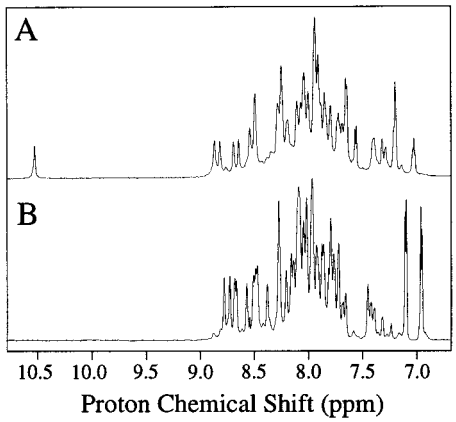

FIGURE 3: One-dimensional ^{1}H NMR spectra of (A) α_3W^1 and (B) α_3Y^1 displaying the amide and aromatic resonances. The spectra were obtained on an Inova 600 NMR spectrometer at 35 °C by using a 12 ppm acquisition window and signal average for 64 scans.

and α_3Y^1 backbones reside in ordered environments. Some of the protons associated with the aromatic side chains in α_3W^1 and α_3Y^1 are easily observable in Figure 3. The narrow resonance observed at 10.53 ppm in the α_3W^1 spectrum represents the N−H proton associated with the indole headgroup. On the basis of chemical shift values (*46*, *47*) and NOESY connectivities (see below), the two well-resolved resonances at 7.04 and 6.89 ppm in Figure 3B are assigned to the H2,H6 and H3,H5 tyrosine ring protons, respectively. We conclude that the 1D ^{1}H NMR spectrum of α_3W^1 and of α_3Y^1 shows a single set of resonances with narrow line width and large chemical-shift dispersion that is consistent with a single, highly populated protein conformation.

More critical evidence that the interiors of the synthetic proteins are well-ordered is provided by natural abundance ^{13}C HSQC spectroscopy. Figure 4 shows methyl region expansions of ^{13}C HSQC spectra obtained from α_3W^1 and α_3Y^1, each of which contains 37 methyl groups associated with their aliphatic residues. Figure 4A represents α_3W^1 in 3 M GdnHCl, which is sufficient to essentially completely denature the protein (see Figure 2B). Thus, Figure 4A displays the random coil ^{1}H and ^{13}C chemical shift values of the seven different methyl groups associated with the alanine, valine, leucine, and isoleucine residues of α_3W^1. The figure shows methyl correlations with random-coil values consistent with those of alanine and isoleucine (*47*) in the relatively upfield ^{13}C spectral region. The methyl correlations arising from valine and leucine residues (*47*) are found in the relatively downfield ^{13}C region of the HSQC spectrum. Figure 4 panels B and C display ^{13}C HSQC spectra obtained from α_3W^1 and α_3Y^1, respectively, in their folded states. Since most of the methyl groups of α_3W^1 and α_3Y^1 are designed to, and presumably do, pack within their hydrophobic cores, the spectra in Figure 4B,C reflect the magnetic environment in the interior of the synthetic proteins. If α_3W^1 and α_3Y^1 have ordered three-dimensional structures, we expect to observe up to three different alanine and six different isoleucine methyl correlations, indicating different magnetic environments for each methyl group of these side chains. The three alanine $C^{\beta}H_3$ methyl correlations and the six CH_3 correlations from the three Ile-$C^{\gamma 2}H_3$ and three Ile-$C^{\delta}H_3$ groups are observed in the two spectra. The spectral region that contains the methyl correlations arising from the six valine and eight leucine residues is less resolved owing to the relatively large number of these amino acids in α_3W^1 and α_3Y^1. Nonetheless, 24−26 of the expected 28 ^{1}H−^{13}C cross-peaks can readily be identified in each of the two spectra. Overall, the ^{13}C HSQC spectra are well-resolved, which indicates that their methyl groups reside in unique magnetic surroundings and provides evidence that α_3W^1 and α_3Y^1 have well-defined tertiary structures in solution. Last, the presence of single sets of methyl ^{1}H−^{13}C correlations for each protein suggest that α_3W^1 and α_3Y^1 populate single conformers in solution.

Characterization of the Aromatic Side Chains. Fluorescence spectroscopy was performed to determine whether W_{32} is buried in the interior of α_3W^1, as designed. The dotted line in Figure 5A represents the fluorescence emission from *N*-acetyl-L-tryptophanamide in solution, which has an emission maximum at 352 nm. The solid line in Figure 5A represents the fluorescence spectrum from α_3W^1 in solution at neutral pH. The fluorescence arising from the protein has an emission maximum at 324 nm. The fluorescence blue shift suggests that W_{32} resides in an apolar, buried position (*64*) and is consistent with the model of α_3W^1 shown in Figure 1. Having established that α_3W^1 has a well-defined structure with the tryptophan buried within its interior, we studied the stability of the protein with respect to pH. Figure 5B displays a pH titration of α_3W^1 following its CD intensity at 222 nm and the fluorescence emission maximum from W_{32}. The figure shows that the secondary and tertiary structures of α_3W^1 are robust with respect to pH changes and remain stable over the 4−10 pH range. The decrease in $[\Theta]_{222}$ observed above pH 10 reveals that the secondary structure begins to denature. As α_3W^1 unfolds, the fluorescence emission maximum shifts to longer wavelengths, consistent with the exposure of W_{32} to the bulk medium. The design of the three-helix bundles includes lysine−glutamate pairs intended to form stabilizing salt bridges on the exterior of the proteins (see below). The p*K* of the lysine side chain is about 10.5 in water, which is close to the pH where α_3W^1 starts to lose its structure. The unfolding process is most likely initiated by the deprotonation of the lysines, which breaks the lysine−glutamate salt bridges and destabilizes the protein.

Figure 5B shows that the CD intensity, which reflects the global unfolding of α_3W^1, and the tryptophan fluorescence, which monitors a local unfolding event, follow the same pH dependence. This observation supports the assumption made above that α_3W^1 unfolds according to a two-state model.

Measurements on α_3Y^1 established that Y_{32}, like the tryptophan in α_3W^1, is also shielded from solvent. Tyrosine has an absorption maximum at 275 nm in aqueous solution, which, upon deprotonation of the phenol headgroup, red-shifts to 293 nm (*65*). Titration curves of tyrosine free in solution and of Y_{32} associated with α_3Y^1 are shown in Figure 6A. The titration curves reveal a p*K* of 11.3 for Y_{32} in α_3Y^1, which is 1.2 pH units higher than the p*K* of tyrosine in solution. The observed increase in p*K* is consistent with a tyrosine residing in a position shielded from the bulk medium. This is further examined in Figure 6B, which follows the α_3Y^1 CD ellipticity at 222 nm and the formation of Y_{32}^- as a function of pH. The pH study reveals that the secondary structure of α_3Y^1 is stable from about pH 4 to 10, as shown above for α_3W^1. α_3Y^1 loses its secondary

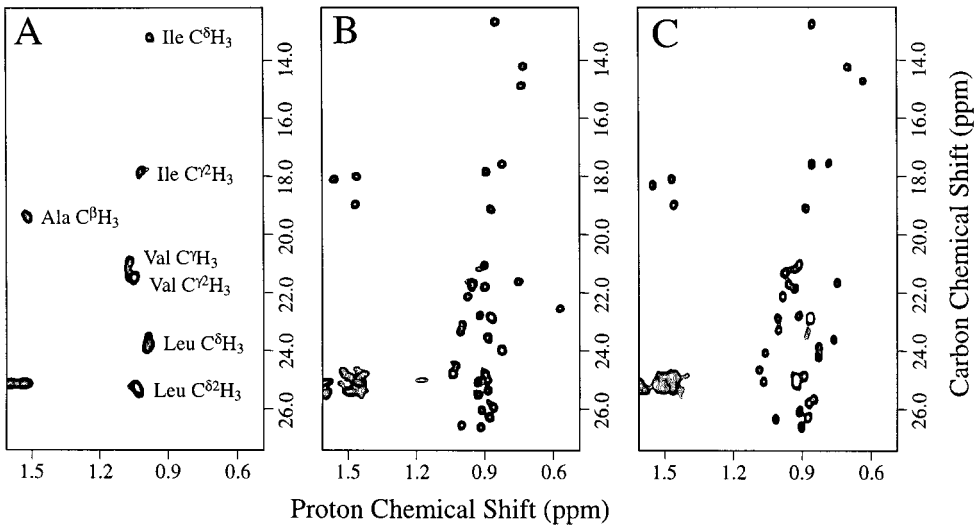

FIGURE 4: Natural abundance ^{13}C HSQC spectra of (A) unfolded α_3W^1 in 3 M GdnHCl, (B) folded α_3W^1, and (C) folded α_3Y^1. These spectra represent expansion of the methyl region and were obtained on an Inova 750 NMR spectrometer under the same conditions as described in Figure 3.

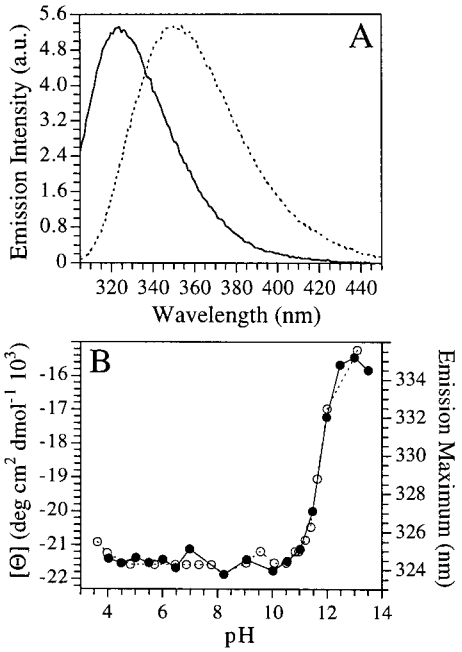

FIGURE 5: (A) Fluorescence spectra from the buried tryptophan in α_3W^1 (solid line) and from *N*-acetyl-L-tryptophanamide in solution (dotted line) obtained on an ISS K2 multifrequency cross-correlation phase and modulation fluorometer. The protein and the tryptophan analogue were dissolved at 15.0 μM in a buffer of 10 mM potassium phosphate and 10 mM KCl, pH 7.0, and placed in a 10 mm path length cuvette. The excitation wavelength was 280 nm and the temperature was 23 °C. (B) Stability of α_3W^1 as a function of pH. The secondary structure was monitored by the CD intensity at 222 nm (●), and changes in the tertiary structure were followed by the tryptophan fluorescence emission maximum (○). The CD measurements were done with 17.5 μM α_3W^1 in a 10 mM potassium phosphate and 10 mM KCl buffer at 25 °C.

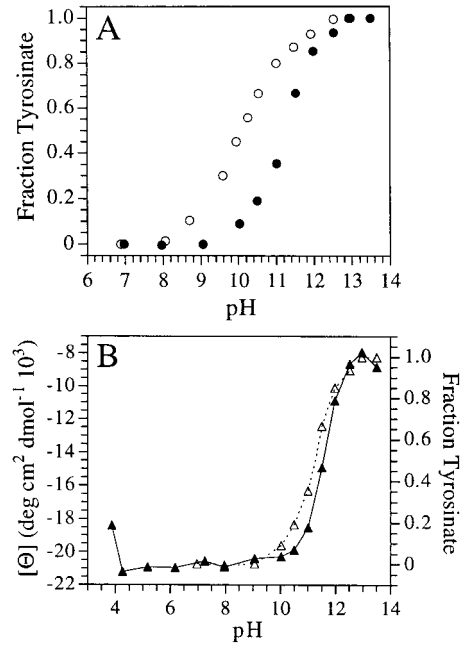

FIGURE 6: (A) pH titration curves from L-tyrosine free in solution (○) and from Y_{32} in α_3Y^1 (●). The titration curves were obtained by monitoring the formation of the tyrosinate species at 293 nm. (B) Stability of the secondary structure of α_3Y^1 as a function of pH as monitored by the CD intensity at 222 nm (▲). The figure also plots the formation of Y_{32}^- as a function of pH (△). The CD measurements were done with 26.0 μM α_3Y^1 in a 10 mM potassium phosphate and 10 mM KCl buffer at 25 °C.

structure concomitant with the deprotonation of the tyrosine, which suggests that these two events are coupled. Thus, at high pH the secondary and tertiary structures are disrupted, exposing Y_{32} to a higher dielectric medium and allowing it to deprotonate. The creation of a charge, in turn, promotes the unfolding process. Consistent with this notion, Figure 6B shows that α_3Y^1 retains about 30% of its α-helical structure at pH 13.5. In contrast, α_3W^1, whose unique tryptophan remains protonated and neutral at this pH, has ∼50% of its secondary structure still intact, as shown in Figure 5B. This suggests that the observed shift of 1.2 pH units in the p*K* of Y_{32} represents the lower limit for the protein-induced change in acidity of this buried residue.

NMR data obtained on α_3W^1 and α_3Y^1 also suggest that their aromatic residues reside within the hydrophobic cores of the respective proteins. Figure 7 shows that nuclear Overhauser enhancements (NOEs) are observed between the protons associated with the aromatic headgroups of W_{32} and Y_{32} and a number of aliphatic protons, including methyl protons. Since the methyl groups are designed to pack in

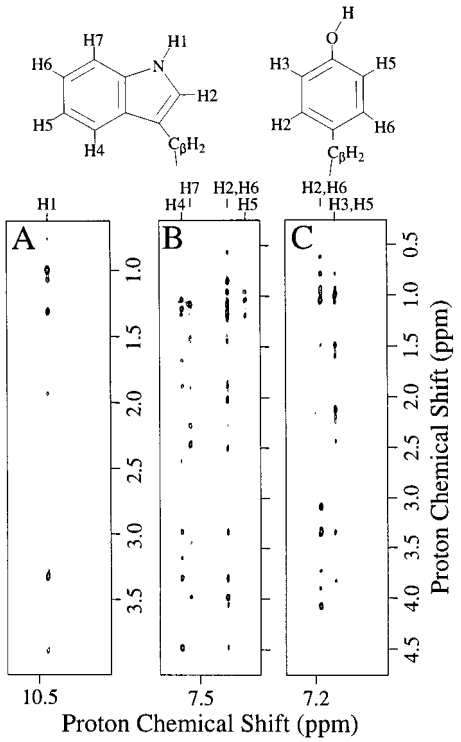

FIGURE 7: Expansions from the NOESY spectrum of (A) α_3W^1 in H_2O showing the NOEs between the indole proton, H1, of W_{32} with nearby (<5 Å) protons. The NOESY spectra of (B) α_3W^1 and (C) α_3Y^1 in D_2O show the NOEs between the aromatic protons of W_{32} and Y_{32} with protons in the close vicinity. The W_{32} H^α, $H^{\beta1}$, $H^{\beta2}$, H2, H4, H5, H6, and H7 resonances are based on the following strong (s), medium (m), or weak (w) NOE correlations: (s) H4−H5, (s) H5−H6, (s) H6−H7, (w) H4−H6, (w) H5−H7, (m) H2−$H^{\beta1}$, (m) H2−$H^{\beta2}$, (w) H2−H^α, (m) H4−$H^{\beta1}$, (m) H4−$H^{\beta2}$, and (m) H4−H^α. The Y_{32} H2 and H6 resonances are assigned on the basis of their strong NOE correlations to the two Y_{32} H^β protons at 3.10 and 3.35 ppm and the Y_{32} H^α proton at 4.08 ppm. The H3 and H5 resonances also show weak NOEs to the Y_{32} H^β protons. The spectra were acquired on a Inova 600 NMR spectrometer under the same conditions as described in Figure 3.

the proteins interior this suggests that W_{32} and Y_{32} are integral with the hydrophobic core. Figure 7A shows the NOESY spectrum from α_3W^1 in H_2O, which displays proton NOEs to the indole H1 proton. Three correlations are observed with chemical shifts <1.1 ppm that represents NOEs between the indole proton and 2−3 different methyl protons. Two additional NOEs with aliphatic resonances at 1.30 and 1.92 ppm are also observed. Figure 7B reveals that the H2, H4, H5, H6, and H7 protons of W_{32} are close to at least eight different methyl protons, assuming that all proton shifts <1.1 ppm arise from methyl protons. Moreover, there are ∼30 additional NOEs observed between the W_{32} aromatic protons and aliphatic resonances with chemical shifts <2.5 ppm. The data shown in Figure 7A,B provide strong support that the whole aromatic headgroup of W_{32} is situated within the hydrophobic core of α_3W^1. The H2,H6 and H3,H5 protons of Y_{32} also show NOEs with at least five different methyl proton resonances and ∼7 additional NOEs to other aliphatic protons with resonances <2.5 ppm (Figure 7C).

In conclusion, the NOESY data obtained from α_3W^1 and α_3Y^1 suggest that their aromatic side chains reside within the hydrophobic cores of these proteins and are consistent with the findings from the fluorescence and optical analyses.

Aggregation State of α_3W^1 and α_3Y^1. Analytical sedimentation equilibrium ultracentrifugation was performed to determine that α_3W^1 is monomeric in solution. A set of data was collected at a protein concentration of 150 μM (not shown) that was well described by assuming a molecular mass of 7440 Da, as expected for a monomer. Furthermore, size-exclusion chromatography on α_3W^1 and α_3Y^1 revealed that the two proteins elute with identical retention times. This result shows that α_3W^1 and α_3Y^1 have similar hydrodynamic radii in solution, which, in turn, suggest that they have the same aggregation state. We conclude that the radical maquettes are monomeric in solution.

Voltammetry Studies on α_3W^1 and α_3Y^1. It has been shown, originally by Harriman (*21*) and later corroborated by DeFelippis et al. (*22*), that electrochemical techniques can be used to estimate the reduction potentials of tryptophan and tyrosine in solution. These species display diffusion-controlled electrode behavior, but no peaks are observed on the reductive scans in their cyclic voltammetry traces (*21*). Irreversible electrochemical oxidation is frequently observed for organic radicals, since these species usually have lifetimes that are short relative to the time scale of the experiment. Although the electrochemical oxidation is not reversible and provides only apparent reduction potentials, the numbers derived from these measurements are in very good agreement with values obtained from pulse radiolysis equilibrium studies (*22*, *66*−*70*).

Figures 8 and 9 show an electrochemical examination of the reduction potentials of tryptophan and tyrosine when dissolved in aqueous buffer and compare them to the potentials of the aromatic side chains in α_3W^1 and α_3Y^1. Figure 8A displays a typical differential pulse voltammogram of the tryptophan derivative *N*-acetyl-L-tryptophanamide. This compound was used instead of L-tryptophan as the solution reference because it allows us to derive the peak potential, E_P, of the indole headgroup without interference from acid/base reactions at the amino and carboxyl groups (C. Tommos and P. L. Dutton, unpublished results). The trace shown in Figure 8A was obtained at pH 1.95 and displays an E_P of 1.07 V and a width at half-height of 0.108 V. For a fully reversible redox reaction with no kinetic complications, the average DPV peak potential approximates the formal reduction potential (*71*). For the irreversible electrochemical measurements reported here, we estimate that $E_P = E_m \pm 0.02$ V (*22*). Under reversible conditions, the width at half-height has been determined to be 0.089 V for an one-electron ($n = 1$) oxidation process at 22 °C (*71*). The broadening of the peak observed in Figure 8A compared to the theoretical value may reflect the fact that the electrochemical oxidation of tryptophan is not reversible. The DPV peak potential of the tryptophan analogue is shown as a function of pH in Figure 8B. In the low-pH region, the peak potential becomes independent of the pH at 1.07 V. In this range we expect that the oxidation reaction produces the tryptophan cation radical; that is, the pH-independent potential represents the $W^{+\bullet}/W$ redox couple. The peak potential titrates with an apparent p*K* of 3.7 and becomes pH-dependent at higher pH with a slope of 0.053 V/pH unit, which is close to the 0.059 V predicted for a H^+/e^- ratio of 1.0. The E_P of the $W^\bullet/W$ redox couple is 0.89 V at pH 7.0. Due to the high p*K* of the indole N−H proton, the pH-independent potential of the $W^\bullet/W^-$ pair is not observed when measuring below pH 14.

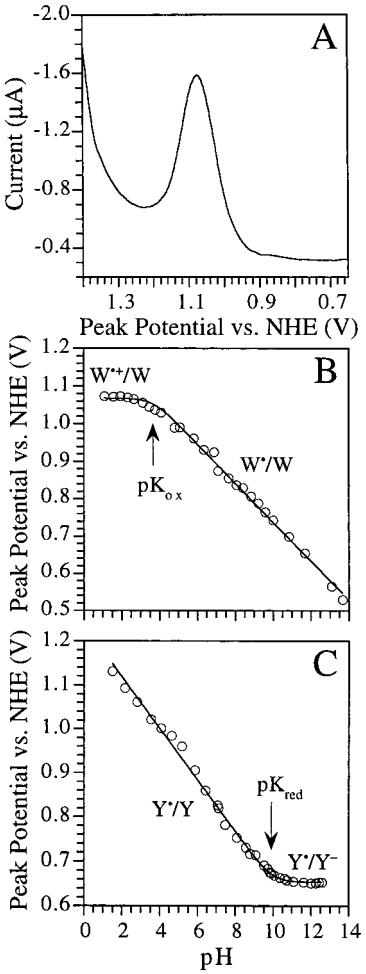

FIGURE 8: (A) Differential pulse voltammogram of *N*-acetyl-L-tryptophanamide at pH 1.95. (B) Peak potentials derived form the differential pulse voltammogram of *N*-acetyl-L-tryptophanamide as a function of pH. The fit to the data is described by $E_P = E_P(W^{\bullet +}/W) + 2.303RT/nF \log (10^{-pH}/(10^{-pH} + 10^{-pK_{ox}}))$, where pK_{ox} represents the $W^{\bullet +} \rightarrow W^{\bullet} + H^+$ reaction. (C) Peak potentials derived from the differential pulse voltammogram of *N*-acetyl-L-tyrosinamide as a function of pH. The fit to the data is described by $E_P = E_P(Y^{\bullet}/Y^-) + 2.303RT/nF \log (1 + 10^{-pH}/10^{-pK_{red}})$, where pK_{red} represents the $Y \rightarrow Y^- + H^+$ reaction. Experimental conditions: compound concentration, 350 μM; scan rate, 10 mV s^{-1}; sample width, 17 ms; pulse amplitude, 50 mV; pulse width, 50 ms; pulse period, 200 ms; quiet time, 4 s; temperature, 22 °C.

A similar set of results was obtained on *N*-acetyl-L-tyrosinamide and is shown in Figure 8C. A pH-independent peak potential of 0.65 V representing the $Y^{\bullet}/Y^-$ redox couple is observed at pH above the p*K* of the reduced tyrosine. From Figure 8C, we obtain a p*K* for the tyrosine derivative of 9.9, which is close to the p*K* of 10.1 derived for L-tyrosine in solution (see above). Below pH 9.9, the potential increases by 0.059 V/pH unit, as predicted. The peak potential of the $Y^{\bullet}/Y$ redox couple is 0.83 V at pH 7. From the data shown in Figure 8C, we estimate that the potential of the tyrosyl cation radical, which has a p*K* of <-2 (*20*), is above 1.35 V. Since these measurements are performed in water, $\sim$1.35 $\pm$ 0.05 V represents the upper limit of the potential window that can be investigated before the solvent itself becomes oxidized (not shown). Thus, the high potential estimated for the $Y^{+\bullet}/Y$ couple is above the range that we can investigate.

As a comparison of the values determined above for the amino acid derivatives, DeFelippis et al. (*22*) reported DPV peak potentials for tryptophan and tyrosine of 1.02 and 0.93 V, respectively, at pH 7.0. Harriman (*21*) obtained the same values for these two amino acids by using cyclic voltammetry. The apparent reduction potentials derived from the electrochemical measurements are in close agreement with the equilibrium E_{m7} values derived from pulse radiolysis studies of 1.03−1.08 V for tryptophan (*66*−*68*) and 0.85−0.94 V for tyrosine (*68*−*70*).

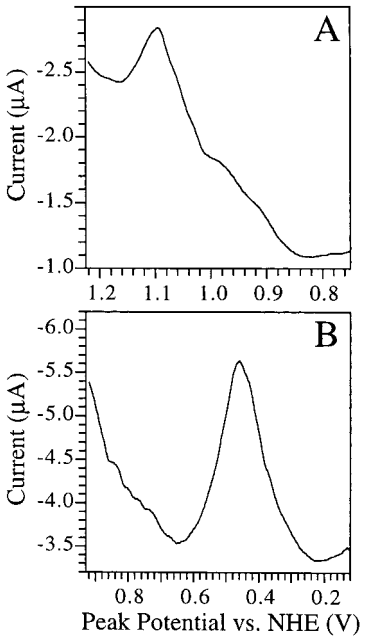

FIGURE 9: Differential pulse voltammogram of (A) α_3W^1 at pH 9.9 and (B) α_3Y^1 at pH 13.4. The protein concentrations were 290 μM for α_3W^1 and 430 μM for α_3Y^1. Experimental conditions: scan rate, 10 mV s^{-1}; sample width, 17 ms; pulse amplitude, 50 mV; pulse width, 50 ms; pulse period, 200 ms; quite time, 4 s; temperature, 22 °C.

Figure 9A shows a DPV trace of α_3W^1 at pH 9.9. The CD and fluorescence data described above show that α_3W^1 is folded under these conditions (see Figure 5B). The α_3W^1 voltammogram displays a peak centered at a potential of 1.09 V with a width at half-height of about 0.080 V. The 1.09 V peak potential derived for α_3W^1 at pH 9.9 is 0.35 V more oxidizing than free tryptophan dissolved in a buffer with similar pH. A shift in peak potential could either arise from a change in reduction potential or reflect a kinetic effect due to an increase in distance between the redox center and the electrode. The small size of α_3W^1, however, prevents any distance effect on the peak potential (*72*). Thus, positioning a tryptophan in an apolar protein milieu raises its reduction potential substantially compared to its solution potential. Moreover, these data indicate that our electrochemical methods are capable of detecting amino acid radicals forming within a folded protein, providing the potential of the side chain occurs in an accessible potential range.

A series of DPV measurements were done on α_3Y^1 starting at alkaline conditions where the protein is largely denatured and its tyrosine deprotonated. Figure 9B displays a DPV trace obtained from α_3Y^1 at pH 13.4. The peak is centered at 0.46 V and has a width at half-height of 0.141 V. This potential corresponds to the $Y_{32}^{\bullet}/Y_{32}^-$ redox couple in a disordered protein/solution environment. As the pH was lowered, permitting α_3Y^1 to fold and bury Y_{32} within its interior, the peak potential shifted toward higher potentials but, concomi-

tantly, the peak amplitude decreased. At pH values below 10.3, where the major portion of α_3Y^1 is folded and its tyrosine is protonated as shown in Figure 6B, a redox response could not be detected from α_3Y^1 (not shown). This suggests that the potential of Y_{32} in the folded α_3Y^1 protein is higher than ~1.35 V, which represents the upper limit that can be investigated before the water solution becomes oxidized. An alternative explanation for the lack of an oxidation wave from the folded protein is that Y_{32} does not make effective electrical contact with the electrode under these conditions. We consider this explanation unlikely, however, since we do detect a response from α_3W^1 in its folded state, as shown above.

The assignment of the electrochemical signals obtained from α_3Y^1 and α_3W^1 to oxidation of their aromatic amino acids is based on several observations. First, no signals were observed in the absence of protein (not shown). Second, α_3W^1 and α_3Y^1 contain no other residues that are expected to have reduction potentials consistent with the signals that we detect, except perhaps for the glycines that form the loops that connect the α-helices in α_3W^1 and α_3Y^1 (see below). We measured glycine free in solution under the same conditions that the protein DPV measurements were performed to verify that these residues were not oxidized electrochemically. The glycine solution did not give rise to any electrochemical response in the potential regions where the protein signals were detected (not shown). Third, the two proteins have amino acid sequences that differ only with respect to their W or Y residue, yet the two proteins gave rise to different DPV traces when studied under the same experimental conditions. This would be expected if the redox-active species changed when the tryptophan in α_3W^1 was replaced by a tyrosine to form α_3Y^1. This observation is also consistent with the conclusion made above that we do not oxidize the glycine loops in the radical maquettes in our electrochemical measurements.

DISCUSSION

The de novo design of proteins represents a recent and potentially very fruitful method to elucidate underlying principles involved in protein structure and function. The basic parameters that determine the formation of secondary structures and the global fold are emerging (*58*−*61*). Although the design of proteins that fold into well-defined tertiary structures remains a significant challenge, clear progress has been made with recent designs (*73*−*80*). As the engineering principles emerge, the introduction of catalytic sites and cofactors that possess various functionalities becomes an increasingly viable prospect. Design of de novo heme proteins has been explored by several research groups (*81*−*85*). The extension of the H10H24 multiheme protein (*81*) to include other metal porphyrins, an iron−sulfur cluster, or flavins demonstrates the possibility of synthesizing proteins that contain multiple redox cofactors (*86*−*89*). Pecoraro, DeGrado, and their collaborators (*90*) have shown other improvements in the design of de novo metalloproteins by constructing mercury-binding sites with defined geometries within the hydrophobic core of α-helical coiled coils. Progress has also been made with respect to the design of proteins supporting various simple functional activities. Baltzer and co-workers (*91*), for example, have developed catalytically active peptides. Electron-transfer reactions across a three-stranded coiled coil in which the N termini were capped with a cobalt ion and the C termini were ligated with viologen complexes have been reported (*92*). Kozlov and Ogawa (*93*) ligated two ruthenium complexes in solvent-exposed positions on opposite sides of a dimeric peptide and observed electron transfer across the peptide−peptide interface. Sharp et al. (*89*) reported light-induced electron transfer between a flavin and a heme that were incorporated into the interior of a synthetic four-helix bundle. Similarly, electron-transfer reactions between a buried heme and a ruthenium complex ligated on the exterior of a four-helix bundle have been observed (*94*). More recently, Shifman et al. (*95*) demonstrated protein-mediated proton exchange coupled to heme oxidation−reduction.

Construction of α_3W^1 *and* α_3Y^1. Here we explore the feasibility of applying the de novo protein design approach to gain a better understanding of side-chain radical chemistry. The aim with the first protein construct was to allow us to recognize and isolate parameters that target a specific side chain for nondestructive redox chemistry within a relatively simple protein setting. We have focused on tryptophan and tyrosine since these amino acids, particularly tyrosine, are found as the redox-active species in many radical enzymes (*4*−*6*). In addition, the aromatic residues have the advantage that both their reduced and oxidized forms are very well characterized, in solution as well as in proteins, by spectroscopic techniques that include optical (*96*−*98*), resonance Raman (*99*), Fourier transform infrared (*100*, *101*), and electron magnetic resonance spectroscopies (*102*−*106*). The radical maquettes are designed as single-stranded proteins containing three α-helices, as shown in Figure 1. The three α-helix motif is common in natural proteins and is found, for example, as the dominating fold in fibrous proteins or as part of a larger structure, as in several DNA-binding proteins (*107*−*109*). The basic α_3 sequence (*32*) used for the radical maquettes was derived from the CoilSer,Val family of synthetic three-helix coiled coils and bundles developed by DeGrado and co-workers over the past decade (*30*, *52*, *74*, *109*−*111*). The sequence of the helix−loop−helix−loop−helix, α_3, peptide contains a total of 65 residues and has a molecular mass of 7.4 kDa. Each helix is designed to contain 19 residues and the three helices are joined by two glycine loops each containing four residues (*32*). The amino acid sequences of α_3W^1 and α_3Y^1 differ only in residue 32, the position of the side-chain cofactor. The core of each protein is designed to contain six hydrophobic layers composed of eight leucines, three isoleucines, six valines, and the aromatic side chain. The exterior positions are occupied by 17 glutamates, 17 lysines, two arginines, and three alanines that are arranged so as to satisfy both intra- and interhelical electrostatic interactions.

In this work a variety of techniques have been used to characterize the structural and thermodynamic properties of the radical maquettes. We have shown that α_3W^1 and α_3Y^1 are monomeric proteins that form thermodynamically stable, well-defined secondary and tertiary structures in solution. Furthermore, their secondary and tertiary folds were shown to be resistant to pH changes, and the proteins remain stable through the physiological pH range. Finally, spectral characteristics and p*K* shifts of their single aromatic side chains suggest that these residues are located within the protein interiors and shielded from the bulk medium, as designed.

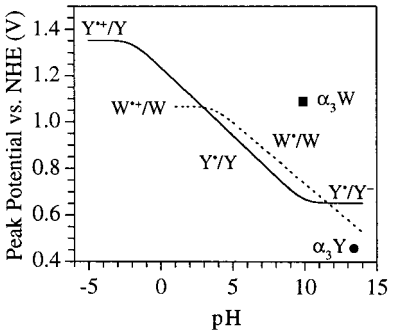

FIGURE 10: Solution potentials of *N*-acetyl-L-tryptophanamide (dotted line) and *N*-acetyl-L-tyrosinamide (solid line) as a function of pH. Also included in the figure are the peak potentials derived from α_3W^1 at pH 9.9 (■) and α_3Y^1 at pH 13.4 (●).

Thus, this work provides strong experimental support for the structural models shown in Figure 1. We conclude that α_3W^1 and α_3Y^1 fulfill the four basic criteria described in the introduction that provide the structural framework for the radical maquettes.

Redox Properties of α_3W^1 and α_3Y^1. Figure 10 compare the electrochemical properties of tryptophan and tyrosine free in solution and when associated with α_3W^1 and α_3Y^1, respectively. The relationship describing the solution potential of tyrosine as a function of pH represents three different oxidation events, which occur in different pH regimes determined by the p*K*s of the reduced and oxidized form of the tyrosine:

$$Y \rightarrow Y^{+\bullet} + e^- \quad (1)$$

$$Y \rightarrow Y^{\bullet} + H^+ + e^- \quad (2)$$

$$Y^- \rightarrow Y^{\bullet} + e^- \quad (3)$$

The pH dependence of the peak potential is described by:

$$E_p = E_p(Y^{\bullet +}/Y) + 2.303RT/nF \log [(10^{-pH} + 10^{-pK_{red}})/(10^{-pH} + 10^{-pK_{ox}})] \quad (4)$$

The redox couple in eq 3 gives rise to the pH-independent potential of 0.65 V observed at pH above the p*K* of the reduced tyrosine, which is 9.9 for *N*-acetyl-L-tyrosinamide. Equation 2 describes the pH-dependent part of the relationship observed below pH 9.9 in Figure 10. Also included in the figure is the potential estimated for the $Y^{+\bullet}/Y$ redox couple. This potential was obtained by fitting the data in Figure 8C with eq 4 and assuming a pK_{ox} of -2 for tyrosine (*20*). A similar relationship describes the tryptophan solution potential as follows:

$$W \rightarrow W^{+\bullet} + e^- \quad (5)$$

$$W \rightarrow W^{\bullet} + H^+ + e^- \quad (6)$$

The reaction in eq 5 gives rise to the pH-independent potential of 1.07 V observed at pH below the p*K* of the cation radical, which is 3.7 for *N*-acetyl-L-tryptophanamide. The reaction described in eq 6 gives rise to the pH-dependent potential observed at pH above 3.7. The potential of the $W^{\bullet}/W^-$ redox pair is not included in the figure since pK_{red} of tryptophan is >14.

When a tryptophan or a tyrosine is transferred from an aqueous, high-dielectric medium to a low-dielectric protein milieu, changes in electrostatic interactions between their reduced and oxidized states are expected to significantly influence their potentials. For example, if we consider the following two reactions

$$W \rightarrow W^{+\bullet} + e^- \qquad \text{dielectric} = 80$$

$$\alpha_3W \rightarrow \alpha_3W^{+\bullet} + e^- \qquad \text{dielectric} = 15$$

a simple electrostatic calculation based on the Born model (*112*), assuming a radius of 4 Å for tryptophan, estimates that the potential of the $W^{+\bullet}/W$ redox couple is raised ~0.2 V when the tryptophan is transferred from a dielectric medium of 80 to a dielectric of 15. The potential of the $W^{+\bullet}/W$ pair will increase further if the dielectric strength is lower than 15 in the interior of α_3W^1. In contrast, if the oxidation occurs as a charge-neutral process, $\alpha_3W \rightarrow \alpha_3W^{\bullet} + H^+ + e^-$, the dielectric property of the medium surrounding the tryptophan is expected to influence its potential to a much lesser extent.

The tryptophan in α_3W^1 gave rise to a peak potential of 1.09 V at pH 9.9, as shown in Figure 10. This value is 0.35 V more oxidizing than the solution E_P obtained for the $W^{\bullet}/W$ redox couple at the same pH. Thus, the potential of the buried tryptophan in α_3W^1 is raised substantially as compared to the solution potential, which clearly suggests that electrostatic interactions are involved in the redox reaction. One possibility for this striking effect is that the side-chain radical formed in this protein is a cation. Alternatively, and more likely, the tryptophan deprotonates during the oxidation but the indole proton remains in the vicinity of the aromatic side chain during the redox cycle. In other words, α_3W^1 does not electrostatically relax the proton into the bulk phase during the lifetime of the radical, which raises the potential of the tryptophan contained within the protein. Potential proton acceptors within α_3W^1 include internal water, the carbonyl groups associated with the protein backbone, and the glutamate residues located in the more solvent-exposed positions.

Y_{32} could be electrochemically oxidized in the unfolded α_3Y^1 protein under conditions where the tyrosine was deprotonated and in contact with the solvent. The peak potential of the $Y_{32}^{\bullet}/Y_{32}^-$ redox couple at pH 13.4 was found to be remarkably low, only 0.46 V. This value is 0.19 V lower than the solution potential of the $Y^{\bullet}/Y^-$ pair, as shown in Figure 10. To our knowledge, the 0.46 V potential observed here for the $Y_{32}^{\bullet}/Y_{32}^-$ couple is the lowest potential reported for tyrosine. There is one example of a covalently modified tyrosine that has a similar low potential. The redox-active tyrosine in galactose oxidase is cross-linked to a cysteine, which forms a thioether bond to one of the *ortho* carbons in the phenol ring. The reduction potential of the thiol-substituted tyrosine has been estimated to be about 0.4 V (*113*, *114*).

The low potential observed for Y_{32}^- in unfolded α_3Y^1 most likely arises from electrostatic effects. α_3Y^1 contains 17 glutamates, 17 lysines, and two arginines, all of which are expected to be deprotonated at pH 13.4. Accordingly, at this alkaline pH the peptide will contain 17 negative charges associated with the deprotonated glutamates in addition to

the tyrosinate at position 32. The electrostatic environment generated by the glutamates is expected to destabilize the reduced tyrosinate form relative to the oxidized neutral radical and consequently lower the potential of the $Y_{32}^{\bullet}/Y_{32}^{-}$ redox pair. Once α_3Y^1 was folded and its tyrosine enclosed within the hydrophobic core, the tyrosine potential became higher than approximately 1.35 V and could not be measured. Nonetheless, the pH-induced unfolding/folding of α_3Y^1 allowed examination of the electrochemical properties of the tyrosine as a function of large-scale changes in its local environment. These results showed that when Y_{32} was moved from a highly charged, disordered protein/solution milieu at pH 13.4 to an ordered, apolar protein environment at pH = 10.3, the potential of the aromatic side chain increased about 0.9 V or more.

The patterns of ^1H and ^{13}C chemical shifts observed in the α_3Y^1 and α_3W^1 ^{13}C HSQC spectra shown in Figure 4 indicate that the hydrophobic cores of these proteins are structurally similar. Consequently, it is reasonable to assume that that their aromatic side chains reside in similar environments. Regardless, the tryptophan in α_3W^1 gave rise to a peak potential of 1.09 V under conditions in which the potential of the tyrosine in α_3Y^1 was too high to measure. Overall, these results provide an experimental demonstration that the reduction potential of tryptophan and tyrosine can be raised considerably when they are moved from a solution environment to an ordered protein milieu. Furthermore, when tryptophan and tyrosine reside in similar hydrophobic protein environments, the potentials of the these side chains differ by $\geq$0.26 V, with the tyrosine being the more oxidizing species. The observed increase in potential for the aromatic residues when residing within a protein, relative to solution values, may be due to a lack of an effective deprotonation mechanism of the aromatic residues in α_3W^1 and α_3Y^1. The protein introduces a kinetic barrier, which prevents or impedes deprotonation of W_{32} or Y_{32} on the time scale of electron transfer. The formation of a charge is expected to affect α_3Y^1 to a greater extent owing to the high reduction potential of the $Y^{\bullet +}/Y$ redox couple, as shown in Figure 10. There are several studies that show that the presence of a proton acceptor is essential to lower the potential of tyrosine contained within a protein. The two redox-active tyrosines in photosystem II, Y_Z and Y_D, are both hydrogen-bonded to nearby histidines, which are essential for radical formation in this enzyme (*115*−*121*). Debus and co-workers (*119*, *120*), for example, have shown that in mutants in which D1-H190 was replaced by a range of other amino acids the oxidation time of Y_Z is lowered from microseconds to milliseconds and the radical yield is decreased dramatically. Similar results were reported by Mamedov et al. (*121*). It was also shown that the microsecond oxidation rate of Y_Z could be restored in the D1-H190 mutants if a high concentration of an external base, like imidazole, was added to the bulk medium (*120*). Blomberg et al. (*122*) used ab initio calculations to investigate the ionization potential, IP, of tyrosine as a function of its local environment. This study showed that the IP was decreased significantly when the tyrosine was hydrogen-bonded to a histidine. The IP was decreased further by introducing a hydrogen-bonding chain. It was also shown that the IP was modulated by the basicity of the hydrogen-bonding network. When a stronger base was included in the calculations, the tyrosine IP became lower. Interestingly, the enzymes that contain redox-active tyrosines all involve neutral radicals (*4*−*6*). Thus far, a catalytically active tyrosyl cation radical has not been experimentally observed.

In conclusion, to develop a protein that efficiently lowers the potential of a sequestered tryptophan or tyrosine, both an electron as well as a proton acceptor should be taken into account. Considerations along these lines will be explored in the development of the next generation of radical maquettes.

ACKNOWLEDGMENT

We are grateful to Professor DeGrado and co-workers for providing the basic α_3 design information prior to publication. We acknowledge valuable discussions with Drs. Gerald Babcock, Brian Gibney, Jonas Johansson, and Chris Moser, and we thank Dr. Jim Lear for assistance with the equilibrium ultracentrifugation measurements. Mass spectroscopic analyses were performed by the Protein Chemistry Laboratory of the University of Pennsylvania.

REFERENCES

1. Reichard, P., and Ehrenberg, A. (1983) *Science 221*, 514−519.
2. Frey, P. A. (1990) *Chem. Rev. 90*, 1343−1357.
3. Klinman, J. P., and Mu, D. (1994) *Annu. Rev. Biochem. 63*, 299−344.
4. Sigel, H., and Sigel, A. (1994) *Metalloenzymes Involving Amino Acid-Residue and Related Radicals*, Marcel Dekker Inc., New York.
5. Babcock, G. T., Espe, M., Hoganson, C., Lydakis-Simantiris, N., McCracken, J., Shi, W., Styring, S., Tommos, C., and Warncke, K. (1997) *Acta Chem. Scand. 51*, 533−540.
6. Stubbe, J., and van der Donk, W. A. (1998) *Chem. Rev. 98*, 705−762.
7. Sjöberg, B.-M., Reichard, P., Gräslund, A., and Ehrenberg, A. (1977) *J. Biol. Chem. 252*, 536−541.
8. Ostermeier, C., Harrenga, A., Ermler, U., and Michel, H. (1997) *Proc. Natl. Acad. Sci. U.S.A. 94*, 10547−10553.
9. Yoshikawa, S., Shinzawa-Itoh, K., Nakashima, R., Yaono, R., Yamashita, E., Inoue, N., Yao, M., Fei, M. J., Libeu, C. P., Mizushima, T., Yamaguchi, H., Tomizaki, T., and Tsukihara, T. (1998) *Science 280*, 1723−1729.
10. Proshlyakov, D. A., Pressler, M. A., and Babcock, G. T. (1998) *Proc. Natl. Acad. Sci. U.S.A. 95*, 8020−8025.
11. Poulos, T. L., and Kraut, J. (1980) *J. Biol. Chem. 255*, 8199−8205.
12. Nordlund, P., Sjöberg, B.-M., and Eklund, H. (1990) *Nature 345*, 593−598.
13. Ito, N., Phillips, S. E. V., Yadav, K. D. S., and Knowles, P. F. (1994) *J. Mol. Biol. 238*, 794−814.
14. Fieschi, F., Torrents, E., Toulokhonova, L., Jordan, A., Hellman, U., Barbe, J., Gibert, I., Karlsson, M., and Sjöberg, B.-M. (1998) *J. Biol. Chem. 273*, 4329−4337.
15. Griepenburg, U., Blasczyk, K., Kappl, R., Hüttermann, J., and Auling, G. (1998) *Biochemistry 37*, 7992−7996.
16. Broderick, J. B., Duderstadt, R. E., Fernandez, D. C., Wojtuszewski, K., Henshaw, T. F., and Johnson, M. K. (1997) *J. Am. Chem. Soc. 119*, 7396−7397.
17. Ollagnier, S., Mulliez, E., Schmidt, P. P., Eliasson, R., Gaillard, J., Deronzier, C., Bergman, T., Gräslund, A., Reichard, P., and Fontecave, M. (1997) *J. Biol. Chem. 272*, 24216−24223.
18. Babcock, G. T., Barry, B. A., Debus, R. J., Hoganson, C. W., Atamian, M., McIntosh, L., Sithole, I., and Yocum, C. F. (1989) *Biochemistry 28*, 9557−9565.
19. Tommos, C., and Babcock, G. T. (1998) *Acc. Chem. Res. 31*, 18−25.
20. Dixon, W. T., and Murphy, D. (1976) *J. Chem. Soc., Faraday Trans. 2 72*, 1221−1230.
21. Harriman, A. (1987) *J. Phys. Chem. 91*, 6102−6104.

22. DeFelippis, M. R., Murthy, C. P., Broitman, F., Weinraub, D., Faraggi, M., and Klapper, M. H. (1991) *J. Phys. Chem. 95*, 3416−3419.
23. Gilchrist, M. L., Jr., Ball, J. A., Randall, D. W., and Britt, R. D. (1995) *Proc. Natl. Acad. Sci. U.S.A. 92*, 9545−9549.
24. Uhlin, U., and Eklund, H. (1994) *Nature 370*, 533−539.
25. Ekberg, M., Pötsch, S., Sandin, E., Thunnissen, M., Nordlund, P., Sahlin, M., and Sjöberg, B.-M. (1998) *J. Biol. Chem. 273*, 21003−21008.
26. Siegbahn, P. E. M., Eriksson, L., Himo, F., and Pavlov, M. (1998) *J. Phys. Chem. B 102*, 10622−10629.
27. Knappe, J., Elbert, S., Frey, M., and Wagner, A. F. V. (1993) *Biochem. Soc. Trans. 21*, 731−734.
28. Wong, K. K., and Kozarich, J. W. (1994) in *Metalloenzymes Involving Amino Acid-Residue and Related Radicals* (Sigel, H., and Sigel, A., Eds.) pp 279−313, Marcel Dekker Inc., New York.
29. Kraulis, P. J. (1991) *J. Appl. Crystallogr. 24*, 946−950.
30. Lovejoy, B., Choe, S., Cascio, D., McRorie, D. K., DeGrado, W. F., and Eisenberg, D. (1993) *Science 259*, 1288−1293.
31. Edelhoch, H. (1967) *Biochemistry 6*, 1948−1954.
32. Johansson, J. S., Gibney, B. R., Skalicky, J. J., Wand, A. J., and Dutton, P. L. (1998) *J. Am. Chem. Soc. 120*, 3881−3886.
33. Pace, C. N. (1986) *Methods Enzymol. 131*, 266−280.
34. Macura, S., and Ernst, R. R. (1980) *Mol. Phys. 41*, 95−117.
35. Müller, L. (1979) *J. Am. Chem. Soc. 101*, 4481−4484.
36. Bodenhausen, G., and Ruben, D. J. (1980) *Chem. Phys. Lett. 69*, 185−189.
37. Marion, D., Ikura, M., Tschudin, R., and Bax, A. (1989) *J. Magn. Reson. 85*, 393−399.
38. Englander, S. W., and Kallenbach, N. R. (1984) *Q. Rev. Biophys. 16*, 521−655.
39. Holzwarth, G., and Doty, P. (1965) *J. Am. Chem. Soc. 87*, 218−228.
40. Lau, S. Y. M., Taneja, A. K., and Hodges, R. S. (1984) *J. Biol. Chem. 259*, 13253−13261.
41. Cooper, T. M., and Woody, R. W. (1990) *Biopolymers 30*, 657−676.
42. Llinás, M., and Klein, M. P. (1975) *J. Am. Chem. Soc. 97*, 4731−4737.
43. Lau, S. Y. M., Taneja, A. K., and Hodges, R. S. (1984) *J. Chromatogr. 317*, 129−140.
44. Nelson, J. W., and Kallenbach, N. R. (1986) *Proteins: Struct., Funct., Genet. 1*, 211−217.
45. Sönnichsen, F. D., Van Eyk, J. E., Hodges, R. S., and Sykes, B. D. (1992) *Biochemistry 31*, 8790−8798.
46. Wüthrich, K. (1986) *NMR of Proteins and Nucleic Acids*, Wiley, New York.
47. Wishart, D. S., Bigam, C. G., Holm, A., Hodges, R. S., and Sykes, B. D. (1995) *J. Biomol. NMR 5*, 67−81.
48. Wishart, D. S., Sykes, B. D., and Richards, F. M. (1991) *J. Mol. Biol. 222*, 311−333.
49. Myers, J. K., Pace, C. N., and Scholtz, J. M. (1995) *Protein Sci. 4*, 2138−2148.
50. Bai, Y., Milne, J. S., Mayne, L., and Englander, S. W. (1994) *Proteins: Struct., Funct., Genet. 20*, 4−14.
51. Bai, Y., Sosnick, T. R., Mayne, L., and Englander, S. W. (1995) *Science 269*, 192−197.
52. Bryson, J. W., Desjarlais, J. R., Handel, T. M., and DeGrado, W. F. (1998) *Protein Sci. 7*, 1404−1414.
53. Alexander, P., Fahnestock, S., Lee, T., Orban, J., and Bryan, P. (1992) *Biochemistry 31*, 3597−3603.
54. Cedergren, L., Andersson, R., Jansson, B., Uhlén, M., and Nilsson, B. (1993) *Protein Eng. 6*, 441−448.
55. Jackson, S. E., Moracci, M., elMasry, N., Johnson, C. M., and Fersht, A. R. (1993) *Biochemistry 32*, 11259−11269.
56. O'Neil, K. T., Hoess, R. H., Raleigh, D. P., and DeGrado, W. F. (1995) *Proteins: Struct., Funct., Genet. 21*, 11−21.
57. Viguera, A. R., Martínez, J. C., Filimonov, V. V., Mateo, P. L., and Serrano, L. (1994) *Biochemistry 33*, 2142−2150.
58. Bryson, J. W., Betz, S. F., Lu, H. S., Suich, D. J., Zhou, H. X., O'Neil, K. T., and DeGrado, W. F. (1995) *Science 270*, 935−941.
59. Beasley, J. R., and Hecht, M. H. (1997) *J. Biol. Chem. 272*, 2031−2034.
60. Smith, C. K., and Regan, L. (1997) *Acc. Chem. Res. 30*, 153−161.
61. Kohn, W. D., and Hodges, R. S. (1998) *Trends Biotechnol. 16*, 379−389.
62. Ohgushi, M., and Wada, A. (1983) *FEBS Lett. 164*, 21−24.
63. Semisotnov, G. V., Rodionova, N. A., Razgulyaev, O. I., Uversky, V. N., Gripas, A. F., and Gilmanshin, R. I. (1991) *Biopolymers 31*, 119−128.
64. Lakowicz, J. R. (1983) *Principles of Fluorescence Spectroscopy*, Plenum Press, New York.
65. Kretchmer, N., and Taylor, R. (1950) *J. Am. Chem. Soc. 72*, 3291−3292.
66. Merényi, G., Lind, J., and Shen, X. (1988) *J. Phys. Chem. 92*, 134−137.
67. Jovanovic, S. V., Steenken, S., and Simic, M. G. (1991) *J. Phys. Chem. 95*, 684−687.
68. DeFelippis, M. R., Murthy, C. P., Faraggi, M., and Klapper, M. H. (1989) *Biochemistry 28*, 4847−4853.
69. Jovanovic, S. V., Harriman, A., and Simic, M. G. (1986) *J. Phys. Chem. 90*, 1935−1939.
70. Lind, J., Shen, X., Eriksen, T. E., and Merényi, G. (1990) *J. Am. Chem. Soc. 112*, 479−482.
71. Parry, E. P., and Osteryoung, R. A. (1965) *Anal. Chem. 37*, 1634−1637.
72. Tender, L., Carter, M. T., and Murray, R. W. (1994) *Anal. Chem. 66*, 3173−3181.
73. Struthers, M. D., Cheng, R. P., and Imperiali, B. (1996) *Science 271*, 342−345.
74. Ogihara, N. L., Weiss, M. S., DeGrado, W. F., and Eisenberg, D. (1997) *Protein Sci. 6*, 80−88.
75. Fezoui, Y., Connolly, P. J., and Osterhout, J. J. (1997) *Protein Sci. 6*, 1869−1877.
76. Schafmeister, C. E., LaPorte, S. L., Miercke, L. J. W., and Stroud, R. M. (1997) *Nat. Struct. Biol. 4*, 1039−1045.
77. Dahiyat, B. I., and Mayo, S. L. (1997) *Science 278*, 82−87.
78. Ilyina, E., Roongta, V., and Mayo, K. H. (1997) *Biochemistry 36*, 5245−5250.
79. Hill, R. B., and DeGrado, W. F. (1998) *J. Am. Chem. Soc. 120*, 1138−1145.
80. Skalicky, J. J., Gibney, B. R., Rabanal, F., Bieber-Urbauer, R. J., Dutton, P. L., and Wand, A. J. (1999) *J. Am. Chem. Soc. 121*, 4941−4951.
81. Robertson, D. E., Farid, R. S., Moser, C. C., Urbauer, J. L., Mulholland, S. E., Pidikiti, R., Lear, J. D., Wand, A. J., DeGrado, W. F., and Dutton, P. L. (1994) *Nature 368*, 425−432.
82. Choma, C. T., Lear, J. D., Nelson, M. J., Dutton, P. L., Robertson, D. E., and DeGrado, W. F. (1994) *J. Am. Chem. Soc. 116*, 856−865.
83. Rau, H. K., and Haehnel, W. (1996) *Ber. Bunsen-Ges. Phys. Chem. 100*, 2052−2056.
84. Rojas, N. R. L., Kamtekar, S., Simons, C. T., McLean, J. E., Vogel, K. M., Spiro, T. G., Farid, R. S., and Hecht, M. H. (1997) *Protein Sci. 6*, 2512−2524.
85. Nastri, F., Lombardi, A., D'Andrea, L. D., Sanseverino, M., Maglio, O., and Pavone, V. (1998) *Biopolymers 47*, 5−22.
86. Rabanal, F., DeGrado, W. F., and Dutton, P. L. (1996) *J. Am. Chem. Soc. 118*, 473−474.
87. Gibney, B. R., Mulholland, S. E., Rabanal, F., and Dutton, P. L. (1996) *Proc. Natl. Acad. Sci. U.S.A. 93*, 15041−15046.
88. Sharp, R. E., Diers, J. R., Bocian, D. F., and Dutton, P. L. (1998) *J. Am. Chem. Soc. 120*, 7103−7104.
89. Sharp, R. E., Moser, C. C., Rabanal, F., and Dutton, P. L. (1998) *Proc. Natl. Acad. Sci. U.S.A. 95*, 10465−10470.
90. Dieckmann, G. R., McRorie, D. K., Tierney, D. L., Utschig, L. M., Singer, C. P., O'Halloran, T. V., Penner-Hahn, J. E., DeGrado, W. F., and Pecoraro, V. L. (1997) *J. Am. Chem. Soc. 119*, 6195−6196.
91. Balzer, L. (1998) *Curr. Opin. Struct. Biol. 8*, 466−470.
92. Mutz, M. W., McLendon, G. L., Wishart, J. F., Gaillard, E. R., and Corin, A. F. (1996) *Proc. Natl. Acad. Sci. U.S.A. 93*, 9521−9526.

93. Kozlov, G. V., and Ogawa, M. Y. (1997) *J. Am. Chem. Soc. 119*, 8377−8378.
94. Rau, H. K., DeJonge, N., and Haehnel, W. (1998) *Proc. Natl. Acad. Sci. U.S.A. 95*, 11526−11531.
95. Shifman, J. M., Moser, C. C., Karlbeck, W. A., Bocian, D. F., and Dutton, P. L. (1998) *Biochemistry 37*, 16815−16827.
96. Land, E. J., Porter, G., and Strachan, E. (1961) *Trans. Faraday Soc. 57*, 1885−1893.
97. Bent, D. V., and Hayon, E. (1975) *J. Am. Chem. Soc. 97*, 2612−2619.
98. Candeias, L. P., Turconi, S., and Nugent, J. H. A. (1998) *Biochim. Biophys. Acta 1363*, 1−5.
99. Backes, G., Sahlin, M., Sjöberg, B.-M., Loehr, T. M., and Sanders-Loehr, J. (1989) *Biochemistry 28*, 1923−1929.
100. MacDonald, G. M., Bixby, K. A., and Barry, B. A. (1993) *Proc. Natl. Acad. Sci. U.S.A. 90*, 11024−11028.
101. Berthomieu, C., Boullais, C., Neumann, J.-M., and Boussac, A. (1998) *Biochim. Biophys. Acta 1365*, 112−116.
102. Sealy, R. C., Harman, L., West, P. R., and Mason, R. P. (1985) *J. Am. Chem. Soc. 107*, 3401−3406
103. Tommos, C., Tang, X.-S., Warncke, K., Hoganson, C. W., Styring, S., McCracken, J., Diner, B. A., and Babcock, G. T. (1995) *J. Am. Chem Soc. 117*, 10325−10335.
104. Hulsebosch, R. J., van den Brink, J. S., Nieuwenhuis, S. A. M., Gast, P., Raap, J., Lugtenburg, J., and Hoff, A. J. (1997) *J. Am. Chem. Soc. 119*, 8685−8694.
105. Huyett, J. E., Doan, P. E., Gurbiel, R., Houseman, A. L. P., Sivaraja, M., Goodin, D. B., and Hoffman, B. M. (1995) *J. Am. Chem. Soc. 117*, 9033−9041.
106. Lendzian, F., Sahlin, M., MacMillan, F., Bittl, R., Fiege, R., Pötsch, S., Sjöberg, B.-M., Gräslund, A., Lubitz, W., and Lassmann, G. (1996) *J. Am. Chem. Soc. 118*, 8111−8120.
107. Lupas, A. (1996) *Trends Biochem. Sci. 21*, 375−382.
108. Kohn, W. D., Mant, C. T., and Hodges, R. S. (1997) *J. Biol. Chem. 272*, 2583−2586.
109. Schneider, J. P., Lombardi, A., and DeGrado, W. F. (1998) *Folding Des. 3*, R29−R40.
110. O'Neil, K. T., and DeGrado, W. F. (1990) *Science 250*, 646−651.
111. Betz, S. F., Bryson, J. W., Passador, M. C., Brown, R. J., O'Neil, K. T., and DeGrado, W. F. (1996) *Acta Chem. Scand. 50*, 688−696.
112. Rich, P. R., Meunier, B., Mitchell, R., and Moody, A. J. (1996) *Biochim. Biophys. Acta 1275*, 91−95.
113. Hamilton, G. A., Adolf, P. K., de Jersey, J., DuBois, G. C., Dyrkacz, G. R., and Libby, R. D. (1978) *J. Am. Chem. Soc. 100*, 1899−1912.
114. Johnson, J. M., Halsall, H. B., and Heineman, W. R. (1985) *Biochemistry 24*, 1579−1585.
115. Tommos, C., Davidsson, L., Svensson, B., Madsen, C., Vermaas, W., and Styring, S. (1993) *Biochemistry 32*, 5436−5441.
116. Tang, X.-S., Chisholm, D. A., Dismukes, G. C., Brudvig, G. W., and Diner, B. A. (1993) *Biochemistry 32*, 13742−13748.
117. Campbell, K. A., Peloquin, J. M., Diner, B. A., Tang, X.-S., Chisholm, D. A., and Britt, R. D. (1997) *J. Am. Chem. Soc. 119*, 4787−4788.
118. Roffey, R. A., Kramer, D. M., Govindjee, and Sayre, R. T. (1994) *Biochim. Biophys. Acta 1185*, 257−270.
119. Chu, H.-A., Nguyen, A. P., and Debus, R. J. (1995) *Biochemistry 34*, 5839−5858.
120. Hays, A.-M. A., Vassiliev, I. R., Golbeck, J. H., and Debus, R. J. (1998) *Biochemistry 37*, 11352−11365.
121. Mamedov, F., Sayer, R. T., and Styring, S. (1998) *Biochemistry 37*, 14245−14256.
122. Blomberg, M. R. A., Siegbahn, P. E. M., and Babcock, G. T. (1998) *J. Am. Chem. Soc. 120*, 8812−8824.

BI990609G